Refined damage prediction of low-rise building envelope under high wind load

F. Pan[1], C.S. Cai[*1], W. Zhang[1,2] and B. Kong[1]

[1]*Department of Civil and Environmental Engineering, Louisiana State University, Baton Rouge, Louisiana 70803, USA*
[2]*Department of Civil and Environmental Engineering, Univ. of Connecticut, Storrs, CT 06269-3037, USA*

Abstract. Since low-rise residential buildings are the most common and vulnerable structures in coastal areas, a reliable prediction of their performance under hurricanes is necessary. The present study focuses on developing a refined finite element model that is able to more rigorously represent the load distributions or redistributions when the building behaves as a unit or any portion is overloaded. A typical 5:12 sloped low-rise residential building is chosen as the prototype and analyzed under wind pressures measured in the wind tunnel. The structural connections, including the frame-to-frame connections and sheathing-to-frame connections, are modeled extensively to represent the critical structural details that secure the load paths for the entire building system as well as the boundary conditions provided to the building envelope. The nail withdrawal, the excessive displacement of sheathing, the nail head pull-through, the sheathing in-plane shear, and the nail load-slip are found to be responsible for the building envelope damage. The uses of the nail type with a high withdrawal capacity, a thicker sheathing panel, and an optimized nail edge distance are observed to efficiently enhance the building envelope performance based on the present numerical damage predictions.

Keywords: low rise; buildings; hurricane; wind tunnel; finite element

1. Introduction

Hurricane-induced economic losses, around $5 billion annually have far outweighed the loss caused by earthquakes and other natural hazards (Pinelli *et al.* 2004). Low-rise residential buildings, the most common buildings in coastal areas, have been repeatedly witnessed as the most vulnerable structures after strong windstorms. The complexity of the highly turbulent wind in the lowest part of the atmospheric boundary layer and the limited knowledge on the structural responses make it difficult to understand the capabilities of those non-fully engineered structures to resist wind loads. Typical low-rise residential buildings are designed using a conventional procedure that treats a building system as a few components in two dimensions without considering their realistic three dimensional interactions. Therefore, though supposed to be highly redundant, typical low-rise residential buildings may not sufficiently secure their continuous load paths. Additionally, the building envelope failure is seldom completely incorporated into structural

---

∗Corresponding author, Professor, E-mail: cscai@lsu.edu

evaluations, though it is the most common one due to hurricane winds. A typical damage of envelope components, e.g., roof shingles or sheathing panels, not only allows the rainwater intrusion and causes additional content damages, but also produces flying debris that threatens neighboring buildings. Therefore, both reliable damage predictions and efficient mitigation measures for residential buildings demand a better understanding of the structural responses under realistic hurricane loads, including system responses and component responses.

Finite element modeling (FEM) of low-rise residential buildings is a flexible and promising approach to accounting for the load sharing directly. It can provide a detailed picture of the contribution from each component to the system performance. Much of the previous numerical research was conducted on the quantitative determination of the load-sharing factor that reflects the influences of how a system imparts to a single representative 2D truss member of a truss assembly for the design purpose. The load-sharing ratio is defined as the mean ratio of the maximum combined stress index (CSI) including and excluding the effect of sheathings, where CSI is an index combining the bending stress and axial stress into a single parameter. Cramer *et al.* (2000) found that the load-sharing ratios ranged from 1.06 to 1.24 for typical wood-truss assemblies involving 7 or 21 trusses spaced at 610 mm on center and with spans up to 11 m. When the load is below twice the design load level, most truss members were subjected to a certain level of bending forces, but with substantial superimposed compressive or tensile forces. The parameter, CSI, was studied for L shapes, T shapes and a complex assembly by Gupta and Limkatanyoo (2008). They found that three system effects, namely, reduced applied load effects, truss-to-truss support effects, and stiffer truss effects, were not included in the conventional design procedure, yielding a 6-60% reduction of the maximum CSI for the cases investigated.

Recently, Martin *et al.* (2011) investigated load paths in a complete 3D FE building model. In their study, wall nail connections were simplified by using an equivalent shear modulus corresponding to specific nailing schedules to account for the variation in shear wall stiffness with different edge nail densities. Falk and Itani (1989) reported that this influence was more significant under higher load levels. The roof diaphragm modulus was considered much less sensitive to the nailing schedule since the roof sheathing was not blocked or nailed along the edges as wall sheathing panels (Martin *et al.* 2011). However, the variations of nail reactions are similarly dependent on the nailing schedule considering the enhanced panel integrity provided by H clips. In spite of their adequacy with respects to the load path analysis, the modelling methods of Martin *et al.*, not considering the realistic nailing schedule, cannot provide realistic boundary restraint conditions to the sheathings that are critical to the building envelope performance. Van de Lindt *et al.* (2007) reported that connection details were the key factors to secure continuous load paths and to reduce the loss of building skins (i.e., the roof sheathing). However, the damage prediction of low-rise buildings through FEM analysis was seldom conducted at the level of connection details. A static nonlinear 3D FEM was created to understand the load distributions and internal force flows of a light framed wood building by a collaborative research effort in Canada (Asiz *et al.* 2008). Their failure analysis focused on the uplift reactions of the truss-to-top plate toe nails and the connection that was judged as failed when the distributed uplift loads at a certain nail exceeded its peak force capacity. Thampi *et al.* (2011) further obtained the Von-Mises stress contours by analyzing a detailed nonlinear 3D FEM results under quasi-static wind pressures to compare with a damaged low-rise building hit by a tornado event. In their study, the nail connections and sheathing panels were modeled in depth but limited details of the modeling were reported.

The rationale of this investigation is to develop a refined analytical methodology, built upon previous research, to more accurately model the structural responses of a typical low-rise

residential building under hurricane loads. There are three primary objectives, namely, to incorporate (1) three dimensional system effects, including but not limited to the truss assembly, (2) the realistic sheathing panel size and placement without overestimating the diaphragm stiffness, and (3) the common nailing schedules employed in the field construction, which provides realistic boundary conditions to the sheathing panels. It is noteworthy that the proposed refined FEM is also promising to shed more lights on the structure capability to sustain loads beyond the first member failure. The first member failure was accepted as the limit state in the design concept but has been questioned on its conservatism for residential houses in the wood research community (Cramer *et al.* 2000). It is clear that a structure can still bear more wind loads when damage initiates in the most vulnerable portion, benefited from its substantial redundancies. This conservatism can serve as the safety backup for design but should be quantified rigorously for damage predictions and mitigations. The proposed FEM is an intended tool with the strengths and potentials to fill this critical gap in the current knowledge base regarding where the failure initiates and how it propagates, eventually leading to study the progressive failure of residential houses under hurricane loads.

2. Finite element modeling

2.1 Building geometry and components

The prototype structure used in the present study is a one-story 5:12 pitched gable roof house with the dimensions of 18.3×13.4×3.0 m for length, width, and overhang height, respectively. This house is of the South/Key CBG type and is a representative building defined in the Florida Public Hurricane Loss Model (FPHLM) (Cope 2004). More information pertaining to the geometry details and opening layout is provided by Pan *et al.* (2013). In the present study, the building is modeled as a timber structure since light-framed wood structures account for about 90% of the existing residential house stock and approximately 95% of new homes in the US (Martin *et al.* 2011). A light-framed wood residential building typically consists of lumber frames (e.g., the truss assembly and wall frames), sheathing panels (e.g., roof sheathings and wall sheathings), joint connections (e.g., sheathing-to-lumber connections or lumber-to-lumber connections) and foundation hold-downs as load bearing components.

The general-purpose structural analysis software, ANSYS (2009), is used to develop an analytical model of the selected prototype house. For lumber frames, both truss members and wall studs are represented by two-node linear isotropic beam elements with six degrees of freedom at each node. Both wall sheathings and roof sheathings are modeled using 8-node linear-elastic orthotropic shell elements with six degrees of freedom at each node. While neglecting wall partitions may lead to over predict the shear wall forces by more than 100%, the structural responses in the higher portion of the building remain limited since the shear responses in the roof-to-wall connections are far below their peak resistances as reported by Asiz *et al.* (2008). Therefore, the internal wall partitions are not included here to simplify the modeling. This is also to be consistent with the model used in the wind tunnel test (Pan *et al.* 2013) that provides aerodynamic data for the present and future FEM analysis. The actual discontinuities between sheathing panels are modeled to avoid an overestimation of the diaphragm stiffness. The roof panels are placed in an offset pattern, that is, the edges of the roof sheathings in the direction parallel to the roof truss are staggered to be more realistic. Furthermore, this panel-by-panel

modeling manner allows more realistically modeling two separate rows of nails on the common border of two neighboring panels.

For nail connections, there are about 34 typical types in terms of the wood products jointed together and about 12 nail sizes involved in typical building constructions according to International Building Code (IBC 2011). Thampi *et al.* (2011) summarized four nail types to make the connection modeling practical as well as representative and are followed in the present study. The sheathing-to-frame nail spacing is chosen as 152 mm along the panel edges and 305 mm at the intermediate supports according to Section 2304.9.1 N ote b in International Building Code (IBC 2011). In the present study, each nail connection is modeled with three independent COMBIN39 elements to represent the load-displacement relationships in the X, Y, and Z direction, respectively. The COMBIN39 element, a zero-mass nonlinear spring connecting a pair of coincident nodes, were used to track the failure process of the nails, and the load-displacement relationships between the coincident nodes were obtained by the laboratory tests documented by Dao and van de Lindt (2008) and Thampi *et al.* (2011). For foundation hold-down devices, the sole plates are rigidly connected to the foundation in this study. Thus, a continuous load path is formed to transfer the wind loads from the building envelope to the foundation.

In the present study, the interior truss configuration was chosen as the "5/12 fink" configuration listed as one of the six typical truss types by Cramer *et al.* (2000) while the gable end trusses were modelled with the vertical webs spaced at 0.6 m as used by Martin (2010). Both truss members and wall members were lumbers with a cross section of 38×89 mm. The wall studs are spaced at 0.4 m while the roof trusses are spaced at 0.6 m, 1.5 times the stud spacing.   The wall studs at corners consist of 2-2×4 and 1-2×4 studs (with the narrow face toward outside) offset 0.1 m from the wall corner. The sole/head plate consists of 2-2×4 studs that are connected at a 1.2 m interval.

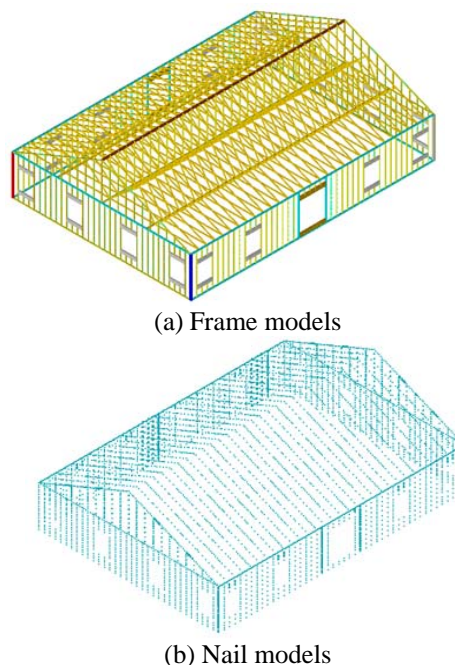(a) Frame models

(b) Nail models

Fig. 1 Sketch of FE model

The framing around doors is strengthened by a nominal 2-2×12 header beam and double studs at both sides. The headers above windows consist of 2-2×10 studs. The ridge board connecting the gable trusses is made of 38 mm×184 mm (known as 2×8) studs.

Finally, 12,811 beam elements, 39,505 shell elements, and 25,428 nonlinear spring elements are created to set up a detailed numerical model with a total DOFs of 849,117. The sketch of the frame members and the nail modeling are shown in Figs. 1(a) and 1(b), respectively.

2.2 Material properties and strengths

All frame and sheathing members are expected to behave in the elastic range. The sources of material properties of both isotropic frame members and orthotropic sheathing panels are mainly from Martin *et al.* (2010), except that the Young's moduli of the truss members were taken from Cramer *et al.* (2000) to match the truss configuration determined by the building floor plan. All the material properties used in the present study are summarized in Table 1. For roof plywood sheathings, an equivalent thickness is used for shell elements instead of the nominal thickness in the bending stress analysis to account for the orthotropic nature of wood, the species groups used for outer and inner plies, and the manufacturing variables involved (APA 1997).

This study is concentrated on a deterministic FEM analysis and variation of material properties are not considered here but will be incorporated in a future stochastic FEM approach to reproduce a more realistic situation. The building envelope damage predicted by the proposed FE model is compared with its counterpart witnessed in real life since the envelope performance has not been completely evaluated before but caused the major economic loss in the past. In fact, the combined failure mechanisms instead of a single one are usually responsible for the observed damage. However, for the sake of simplicity, seven relevant limit states are discussed separately to investigate the impact of the structural component to the envelope performance in the following sections. The seven limit states discussed include three nail connection failure modes (i.e., the nail shank withdrawal from the lumber, the nail head pull-through of the sheathing panel, and the nail load-slip failure) and four sheathing failure modes (i.e., the sheathing panel failure due to the shear stress, the bending stress, the axial forces, and the excessive displacements). Accordingly, the capacity for each limit state defined in design standards is listed in Table 2 as the criteria to judge the building envelope damage discussed in the later "Analysis results" section.

Table 1 Material properties

	Component	Species/size	Young's modulus (GPa)	Shear modulus (GPa)	Poisson's ratio
Isotropic material	Truss top/ bottom chord	38×89 mm southern pine	11.03	-	0.36
	Truss web	38×89 mm spruce-pine-fir	9.72	-	0.36
	Wall Stud	38×89 mm spruce-pine-fir	8.3	-	0.4
Orthotropic material	Roof sheathing	13 mm plywood	13.1/2.0 /2.0	1.0/1.0/1.0	0.08/0.08/0.08
	Wall sheathing	11 mm OSB	5.1/1.6/1.6	0.8/0.8/0.8	0.08/0.08/0.08

Table 2 Allowable stresses for Structure-1 plywood

Structural component	Response	Type of force/stress	Ultimate Capacity / Failure stress	COV %	Sources
Sheathing-to-frame nail	Withdrawal	Axial reactions in nails	38 N/cm [a,b]	28.5	(Herzog and Yeh 2006)
	Nail head pull through	Axial reactions in nails	313 N [c]/227 N [d]	11.7/15.1	(Herzog and Yeh 2006)
	Load-slip	Transvers reactions in nails	988 N [e] /1073 N [f]	-	(Mi 2004)
Sheathing	Axial [g]	Tension/compression in plane of plies	6.76/6.69 MPa	-	(APA 1997)
	Shear [g]	Shear through the thickness/ Rolling shear	1.07/0.43 MPa	-	(APA 1997)
	Bending [g]	Extreme fiber stress in bending	9.86 MPa	-	(APA 1997)
	Disp.	Displacement at the middle span of sheathing panels	1/120L [h]	-	(IBC 2012)[a]

a. 15 mm plywood panels connected to the frame lumber by plain nails (2.5 mm × 57 mm, Senco Product BJ23E) under a dry-dry exposure condition.

b. Nail withdrawal strength within the test range is not sensitive to the panel thickness.

c. 13 mm plywood panels connected to the Southern pine frame lumber under a dry exposure condition by 8d box nails (3mm × 63.5 mm with a head diameter of 7.5 mm).

d. The same as note c except the wet exposure condition (24 hour water soak prior to the test).

e. 11 mm OSB panels connected to 38mm × 89 mm No.2 spruce-pine-fir (SPF) by 63.5 mm 8d common nail connections. Nails were loaded perpendicularly to the grain. The nails were 2d away from the sheathing edge.

f. The same as note e except nails loaded in parallel to the grain.

g. The allowable stresses for plywood of "Structural-1 Grade Stress Level" under "Wet condition" by APA (1997).

h. Table 1604.3 of the 2012 IBC for walls with flexible finishes.

One major source for the capacities of the involved components is APA-the Engineered Wood Association (APA 1997) that has conducted comprehensive tests related to the engineered wood products in a systematic manner. Other available publications (Girhammar *et al.* 2004, Mi 2004, Herzog and Yeh 2006, Dao and van de Lindt 2008 and Thampi *et al.* 2011) served as complementary sources to find the best match for the components in the proposed FE model, and to ensure the appropriate use of resistances for comparison purposes. To the authors' knowledge, there are rare comprehensive reports on the capacities of building components for the entire building system. Instead, most of the past research focuses on the capacities of a specific connection type, lumber size or sheathing grade individually. Since multiple factors may influence the capacity of each type of structural components and may consequently change the damage prediction results, those related factors are documented under each limit state in the later "Analysis Results" section and their impacts are directly discussed with the corresponding numerical prediction.

2.3 Simulated wind loads

Wind pressures are simulated via the wind tunnel tests on a 1:50 scaled model of a one-story 5 on 12 sloped residential building at the Boundary Layer Wind Tunnel of Louisiana State University. The mean wind velocity and turbulence intensity profiles for the open terrain condition are produced as Fig. 2 shows. Totally, 3 internal taps are installed on the inner layer of the double walls and 188 external pressure taps on the outer layer of the model to determine the surface pressures on both sides of the building envelope as shown in Fig. 3. All tap pressures are sampled

by Scanivalve DSA 3217 digital module at a sampling frequency of 500 Hz per channel per second. More details related to the test configuration and instrumentation were reported by Pan *et al*. (2013).

It is noted that in the present study, only the initial failure is concerned and therefore the internal pressure is not considered. It will be used in the on-going progressive failure prediction that will consider the breakings of openings and thus the induced internal pressures. The measured external surface pressures are divided by the mean dynamic pressure $\overline{p}_h$ at the mean roof height h of 4.4 m (full scale) to obtain the time history of pressure coefficient $C_{p,h}(t)$ since this normalization is considered to produce the least variability (Ho *et al*. 2005). The mean pressure coefficients $\overline{C}_{p,h}$ are here used instead of $C_{p,h}(t)$ time series to target the most vulnerable components for the building envelope performance at less computational cost in the following "Analysis Results" section. This simplification is based on the quasi-steady assumption, i.e., the fluctuating pressure on a structure is assumed to follow the variations in the longitudinal wind velocity upstream (Holmes 2001). As a result, the peak pressure on the building surface can be predicted as

$$\hat{p} = (1/2)\rho_a \hat{U}^2 \times \overline{C}_p \tag{1}$$

where, ρ_a is air density, $\overline{C}_p$ is mean pressure coefficient, and $\hat{U}$ is peak gust velocity. The full correlation of pressure peaks is implied in Eq. (1). However, for its application over large areas, Eq. (1) is conservative, since the realistic pressures on the entire building envelope will not reach their peaks simultaneously. Therefore, the reduction is needed. The gust effect factor G is introduced into Eq. (2) for a twofold purpose: to reduce this non-contemporaneous wind action and to account for the resonant amplification of structural responses due to turbulence (Solari and Kareem 1998)

$$p = (1/2)\rho_a \hat{U}_{3s}^{\,2} \times G \times \overline{C}_p \tag{2}$$

where, $\hat{U}_{3s}$ is the maximum 3 second gust wind speed. In ASCE 7-10, $G = 0.85$ is assigned for rigid buildings whose fundamental frequency is not less than 1 Hz (ASCE 2010). Eq. (2) is the basis for the wind load calculations to predict the building envelope damage in the current study. It is noted that G=0.85 is explicitly considered in the present loading calculation because in FEM, the global performance of the structure, considering the interaction between the frames and the sheathings, is concerned. In contrast, C&C loading in ASCE code (ASCE 2010) is for local analysis and a combined GCp is specified.

The mean external wind pressure coefficients $\overline{C}_{p,h}$ based on 4-second measurements range from 97% to 105% of that based on 10-second measurements for taps near the ridgeline, leeward roof edge, and windward wall edges. The contours of the mean external wind pressure coefficient $\overline{C}_{p,h}$ over 10 second measurements are shown on Fig. 4(a) and those mean contours are further discretized for the wind loading input on the refined FE model as illustrated in Fig. 4(b). The applied wind pressures on the developed FE model as calculated by Eq. (3) corresponds to $\hat{U}_{3s,h}^{Open}$, the 3 second gust wind speed at the mean roof height h over the open terrain.

(a) Mean velocity profile

(b) Turbulence intensity profile
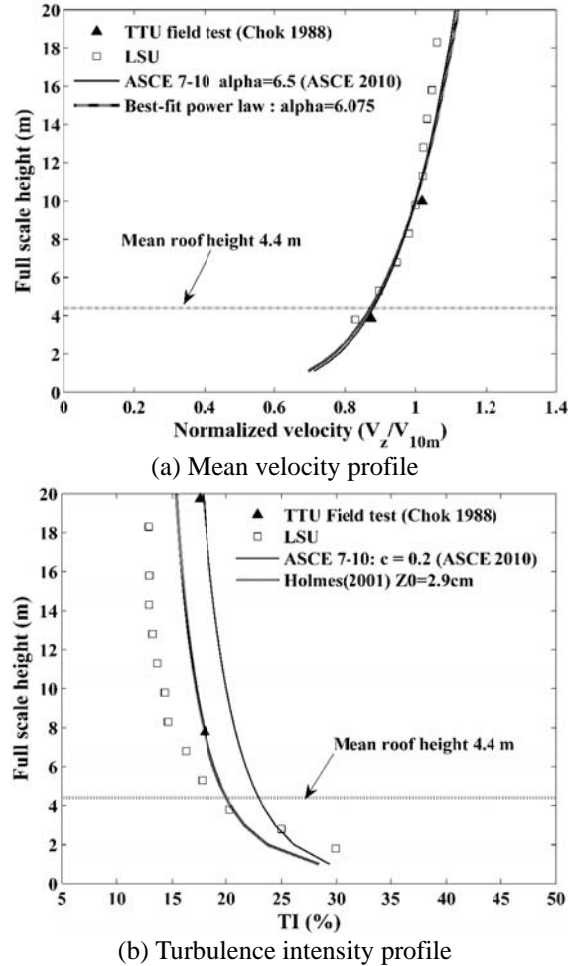
Fig. 2 Wind tunnel mean velocity and turbulence intensity profiles for open exposure

$$p = (1/2)\rho_a (\hat{U}_{3s,h}^{Open})^2 \times 0.85 \times \overline{C}_{p,h} \qquad (3)$$

$\hat{U}_{3s,h}^{Open}$ is then adjusted from 4.4 m to 10 m according to the mean velocity profile to be equivalent to the 3 second gust wind speed at 10 m over the open terrain $\hat{U}_{3s,10m}^{Open}$ that is used in ASCE 7-10. To interpret the predicted structural responses in the "Analysis Results" section in terms of the Saffir-Simpson scale, $\hat{U}_{3s,10m}^{Open}$ is then divided by a conversion factor of 1.09 to obtain 1 minute gust wind speed at 10 m above the open water $V_{1min,10m}^{Water}$ according to Simiu *et al.* (2007). All the conversions among the wind speeds discussed above are tabulated in Table 3 for clarity. The wind speed discussed hereafter is the 3-second gust wind speed while its equivalence in the

Saffir-Simpson scale is denoted in the following parentheses, i.e., $\hat{U}_{3s,10m}^{Open}$ ($V_{1min,10m}^{Water}$). The unit m/s is kept here to be consistent with the SI unit system and it can be converted to mph by multiplying 2.24 for the discussion in the Saffir-Simpson scale.

It is noted that since this study is to demonstrate the damage modeling procedure under a given wind loading, only the external pressure coefficients corresponding to the wind incidence angle of 90˚, i.e., the oncoming flow being perpendicular to the ridge line, were selected. Higher structural responses or lower critical wind speeds are expected when additional wind incidence angles are investigated. For this particular wind incidence angle, the wind speed ranging from 22 to 127 m/s was applied as a scaling factor as implied in Eq. (3) to the proposed model at an increment of 2.24 m/s, i.e., 5 mph. A series of non-linear static analyses were performed to identify the potential damaged areas indicated by the von-Mises stresses and further to evaluate the envelope performance by seven failure limit states. At each wind speed, the nonlinear model was loaded incrementally and solved by a full Newton-Raphson solution procedure where the stiffness matrix is updated in each iteration. Within each load increment, iterations are repeated till the equilibrium is achieved to satisfy the target convergence tolerances of both the force and displacement.

Table 3 Conversions among the involved wind speeds $\hat{U}_{3s,h}^{Open}$, $\hat{U}_{3s,10m}^{Open}$, and $V_{1min,10m}^{Water}$

	$\hat{U}_{3s,h}^{Open}$ (Eq. (3))	$\hat{U}_{3s,10m}^{Open}$ (ASCE 7-10)	$V_{1min,10m}^{Water}$ (Saffir-Simpson scale)
m/s	1	1.14	1.05(=1.14/1.09)
Conversion factor and related parameters	---	Mean velocity profile Fig. 2(a) $\dfrac{U_{10m}}{U_h} = (\dfrac{Z_{10m}}{Z_{4.4m}})^{\frac{1}{6.075}} = 1.14$	$V_{3s,10m}^{Open} / V_{1min,10m}^{Water} = 1.09$, when Exposure C surface roughness is 0.03 m, open-water surface roughness is 0.005 m (Simiu *et al.* 2007)

3. Analysis results

3.1 Von Mises stress outputs

To obtain a quick snapshot of the potential damage locations, the entire model is assumed to sustain wind loads as a unit here. More specifically, any overloaded portion is not removed from the model and the Von Mises stress is chosen as the sole index to reflect the complex three-dimensional stress status throughout the 3D building system. For the isotropic material, the Von Mises stress threshold may have the same magnitude as the axial material strengths, either the tensile or compressive stress. In the present case, the tensile and compressive strength for the roof sheathing panels are 6.76 MPa and 6.69 MPa, respectively. However, reduction factors are introduced in APA's Plywood Design Specification as 1/6 and 1/3 when the axial force is at 45˚ to the face grain for the tension and compression cases, respectively (APA 1997). Therefore, to include the nonhomogeneous characteristics of the sheathing panel, the threshold of 1.13 MPa, 1/6 of the tensile allowable stress, is chosen in the present study to predict and visualize the potential damage areas.

The results show that the Von Mises stresses always start to concentrate at the nail spots where the boundary conditions constrain the deformation of the building envelope and then develop toward the mid-span of the sheathing panels between the frame supports as Fig. 5(a) shows. This indicates that the initial failure modes may be related to the connection details and the subsequent failure modes may involve certain sheathing limit states, i.e., sheathing bending, sheathing shear, or beam buckling. The Von Mises stresses exceed the threshold at the lowest sheathing panel in the leeward roof as well as the windward gable end wall at $\hat{U}_{3s,10m}^{Open} = 51$ m/s ($V_{1min,10m}^{Water} = 47$ m/s).
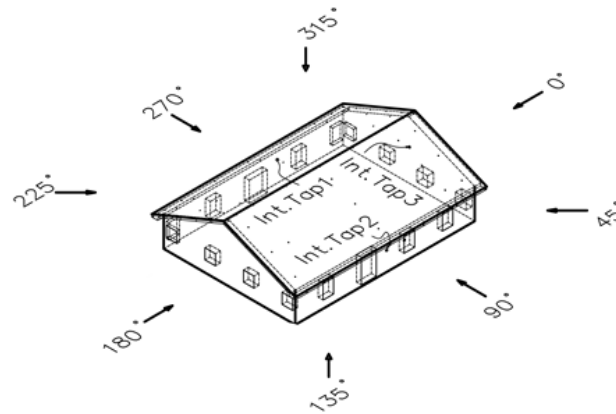

(a) Wind incidence angles

(b) Scaled model details

Fig. 3 1:50 scaled wind tunnel model
(Prototype: $18.3 \times 13.4 \times 3.0$ m Length $\times$ Width $\times$ Overhang Height)

At $\hat{U}^{Open}_{3s,10m} = 88$ m/s ($V^{Water}_{1\min,10m} = 80$ m/s) wind speed, a Category 5 hurricane event, the Von Mises stresses develop significantly at the leeward roof sheathing panels, the windward gable end walls, and the windward wall edges as shown in Fig. 5(b). All those potential damage zones correspond to the wind suction areas of $\overline{C}_p$ contours as shown in Fig. 4(a). It is also noteworthy that those predictions under a single wind attack angle qualitatively agree well with some of the observed failures at roof edge sheathings, gable end walls, and side walls as shown in Figs. 5(c) and 5(d), though they may be caused by wind fields with different attack angles. Those agreements indicate that the proposed refined FEM is able to capture the detailed local damage in addition to the global responses that are typically predicted by most previous simplified FE models, such as displacements and/or reactions at key locations.
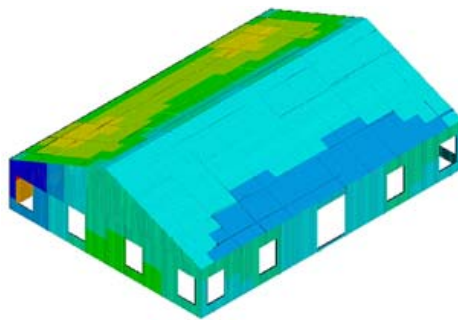

(a) Mean external pressure coefficients $\overline{C}_p$ contours under 90 ° (Refer to Fig.3 (a))
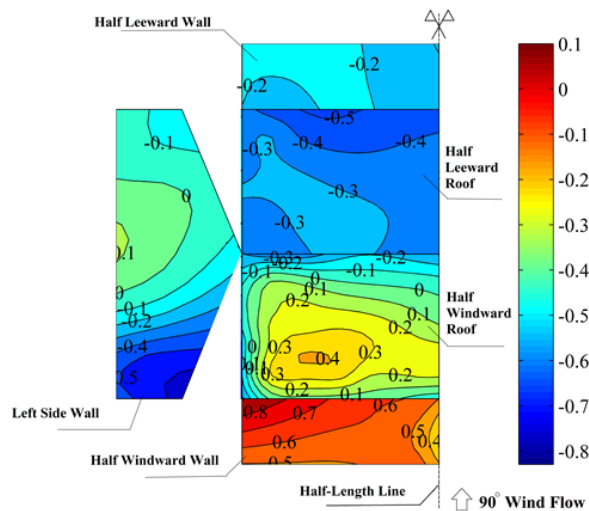

(b) Discretized $\overline{C}_p$ contours under 90° for FE analysis

Fig. 4 Mean wind pressure coefficient contours and their discretization

Further investigations on each of the seven failure modes and the corresponding initial failure wind speed are discussed in the following subsections to link the potential damage areas indicated by the Von Mises stresses to a specific failure mode. No combinations of the seven failure modes are considered here in order to observe how each failure mechanism affects the overall building envelope performance separately.
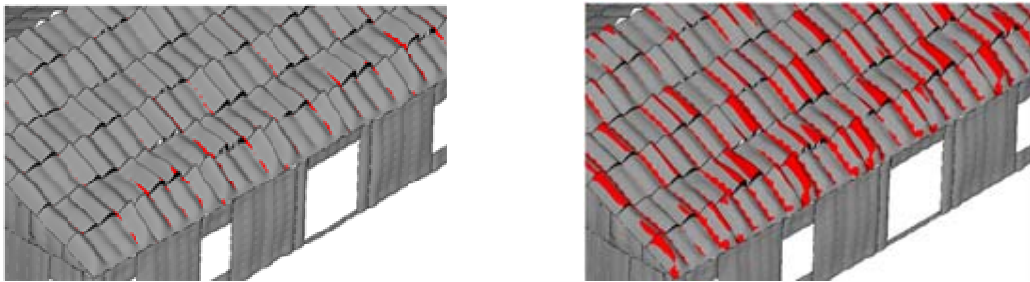
(a) Development of Von Mises stresses from connection spots to mid-span of sheathing panels from $\hat{U}_{3s,10m}^{Open} = 59$ to 85 m/s ($V_{1min,10m}^{Water} = 54$ to 78 m/s)
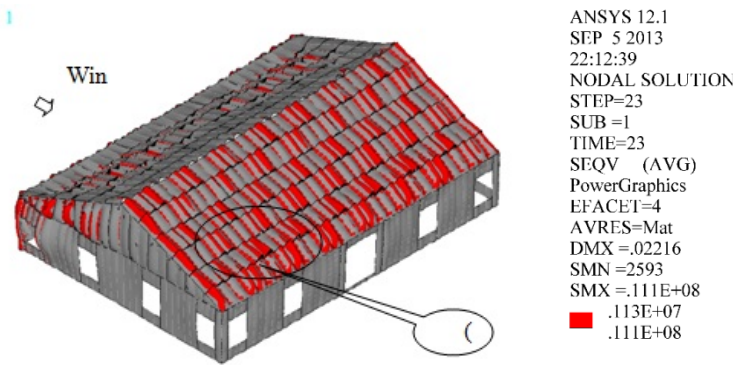
(b) Von Mises stresses at $\hat{U}_{3s,10m}^{Open} = 88$ m/s ($V_{1min,10m}^{Water} = 80$ m/s)

(c) Gable end wall and roof edge sheathing (arrows) failure in Katrina (FEMA 2006)

(d) Gable end and side wall failure in Andrew (FEMA 1992)

Fig. 5 Comparison of predicted potential damage areas and observed building damage

3.2 Displacements

The total displacement of each point on the building envelope consists of two parts, i.e., the local displacement of the cladding supported on the undeformed frame, and the displacements due to the global building frame deformations and the sheathing-to-frame connection elongations or rotations as shown in Fig. 6(a). From Fig. 4(a), it is clear that the windward wall, windward roof, and the leeward part of the side walls sustain compressive pressures while the leeward roof, the windward wall edges, and the leeward wall experience suctions. The lumber frame, including the truss assembly and wall frames, responds to the total wind loads as a unit on the system scale instead of being controlled by the local pressures. For example, the windward wall studs and the wall studs near the windward edges of the side walls are bent outward due to the compressive pressures on the windward roof as shown in Fig. 6(b). The displacements of the sheathing panels between the supports, i.e., the wall studs or the truss frames, are primarily determined by the actions of the local wind pressures. For example, the wall panel displacements between the wall studs on the windward wall are toward inside due to the local compressive pressure in spite of the wall studs are bent outward due to the global deformation under the compressive (positive) surface pressures transferred from the windward roof.

The predicted maximum displacement occurs at the second lowest row of the roof sheathing at the leeward roof when the wind speed is from $\hat{U}_{3s,10m}^{Open} = $ 25 to 74 m/s ($V_{1min,10m}^{Water} = 22$ to 67 m/s), i.e., up to the Category 4 hurricane scale. When the oncoming wind speed exceeds $\hat{U}_{3s,10m}^{Open} = 74$ m/s ($V_{1min,10m}^{Water} = 67$ m/s), i.e., Category 4 and above, the maximum displacement shifts to the side wall sheathing close to the first side window near the windward edge as shown in Fig. 6(a). This indicates that the localized suction determines the envelope response in the low wind speed range while the frame system response to the overall wind loads decides the location of the maximum displacement in the high wind range. The frame system response may be responsible for the maximum displacement at even lower wind speeds in the presence of internal pressures due to the dominant windward openings that will be reported later. At $\hat{U}_{3s,10m}^{Open} = 51$ m/s ($V_{1min,10m}^{Water} = 47$ m/s), the predicted maximum displacements are 6 mm in the low edge sheathing on the leeward roof. If the panel deflection criterion is set as 1/120 of the roof truss span (= 5 mm) in accordance with Table 1604.3 of the 2012 IBC (IBC 2011), the corresponding failure wind speeds are $\hat{U}_{3s,10m}^{Open} = 51$ m/s ($V_{1min,10m}^{Water} = 47$ m/s).

3.3 Nail Withdrawal

The nail withdrawal is one dominant failure mode observed in wood panels when the nail embedment fails (FEMA 2005a). The nail withdrawal resistance is commonly determined by the surface friction that holds an embedded plain shank nail in a structural panel. Additionally, the shear resistance provided by the annularly threaded rings of ring shank nails serves as a mechanical lock that further prohibits the withdrawal and increases the withdrawal capacity by 276 % compared to the plain shank nails under dry conditions (Herzog and Yeh 2006). A reduction factor of 0.75 is recommended by Herzog and Yeh (2006) for the applications exposed to wet service conditions under which a panel is soaked 24 hours before or after the nail installation based

on their laboratory tests. The withdrawal capacities for three types of nails (i.e., plain shank, screw shank, and ring shank nails) connecting either an 13 mm roof plywood sheathing panel or 11 mm wall OSB panel to the lumber frame under dry and wet service conditions range from 92 N to 673 N (Herzog and Yeh 2006) as listed in Table 4. The wind speeds corresponding to the initial nail withdrawal failure for the roof and four exterior walls can be identified once the nail withdrawal reactions are output by the proposed FE model. The first failure wind speeds, i.e., the minimum wind speed initializing a failure, for the entire roof and the entire wall are listed in Table 4 along with the design wind speeds. The design wind speeds correspond to the allowable wall surface pressures determined together by the nail withdrawal capacity, nail head pull-through capacity, and panel capacities (APA 2012).

(a) Total displacement contours in WT load case
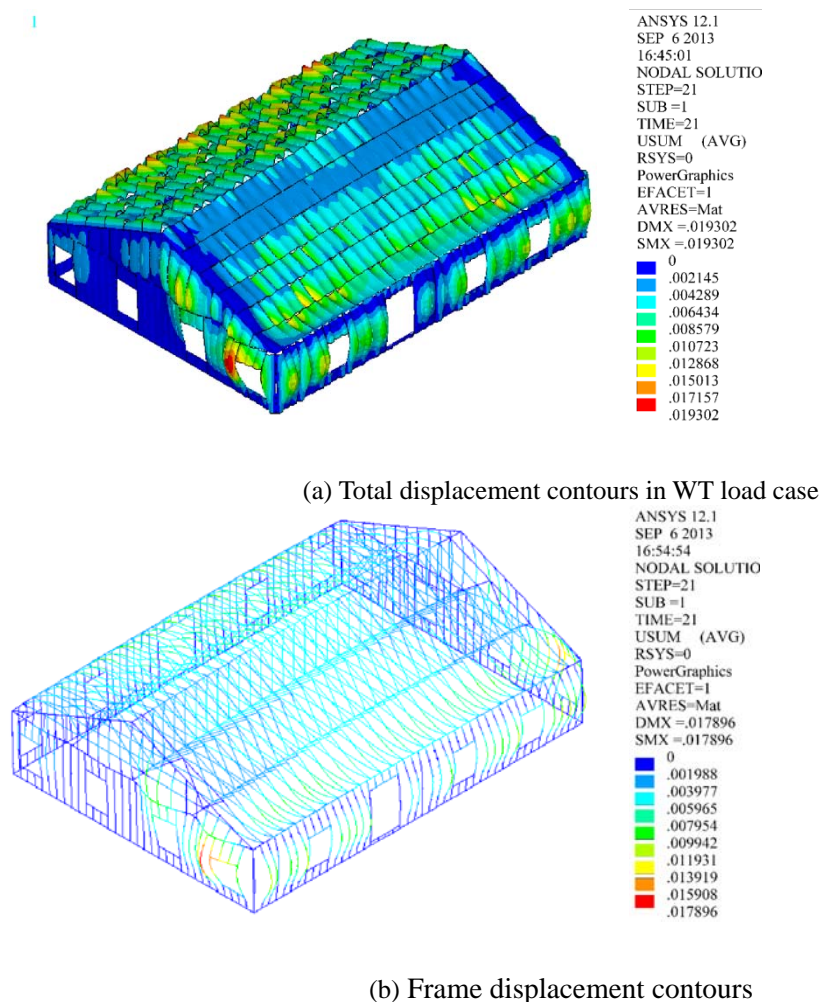

(b) Frame displacement contours

Fig. 6 Displacement contours under wind pressures at $\hat{U}_{3s,10m}^{Open} = 73$ m/s ($V_{1min,10m}^{Water} = 67$ m/s)

The most vulnerable roof nail fails after the most vulnerable wall nail does. As shown in Table 4, a plain shank nail fastening a 13 mm roof panel close to the side edge of the front roof fails at $\hat{U}^{Open}_{3s,10m} = 83$ m/s ($V^{Water}_{1min,10m} = 76$ m/s) under the dry condition. It is 55% higher than $\hat{U}^{Open}_{3s,10m} = 54$ m/s ($V^{Water}_{1min,10m} = 49$ m/s) when the same type connection fails on the corner edge of the leeward wall under the dry condition. On average, the first failure wind speeds for the most vulnerable roof nail are around 154% of those for the most vulnerable wall nail (156%=(170/110+150/95+150/95+130/85)×100%/4, see the "plain shank nail" column in Table 4).

Table 4 Nail withdrawal resistances (R) and corresponding first failure wind speeds

Panel thickness/ service condition	Plain shank nail			Ring shank nail			Screw shank nail			Design wind speed [b] (m/s)
	R [a] (N)	First failure wind speed (m/s)		R (N)	First failure wind speed (m/s)		R (N)	First failure wind speed (m/s)		
		roof	wall		roof	wall		roof	wall	wall
13 mm (1/2") Plywood dry	184	83 (76)[c,d]	54 (49)	673		102 (94)	170	80 (74)	54 (49)	
13 mm (1/2") Plywood wet	138	73 (67)	46 (42)	505	139+ (127+)	88 (80)	127	68 (63)	44 (40)	57 (6d nail) or 66 (8d nail)
11 mm (7/16") OSB dry	138	73 (67)	46 (42)	534		93 (85)	123	68 (63)	44 (40)	
11 mm (7/16") OSB wet	103	63 (58)	42 (38)	400	124 (114)	80 (74)	92	59 (54)	39 (36)	

a. "R" denotes resistance.

b. "Design wind speed" is converted from 3 second gust wind speed at the mean roof height of 9.14 m (30 ft) used in APA (2012) to 10 m to be consistent with ASCE 7-10 wind speed, e.g., 57=56×(10/9.14)$^{(1/6.075)}$.

c. The wind speeds are $\hat{U}^{Open}_{3s,10m}$ ($V^{Water}_{1min,10m}$).

d. 1 m/s= 2.24 mph.

Under both the dry and wet conditions, the first failure wind speeds predicted for the plain shank nails and screw shank nails on walls are lower than the recommended wall design wind speeds. For example, the most vulnerable wall nail that connects the 11 mm OSB wall panel to the lumber frame under the wet condition fails at $\hat{U}^{Open}_{3s,10m} = 42$ m/s ($V^{Water}_{1min,10m} = 38$ m/s), 26% lower than $\hat{U}^{Open}_{3s,10m}$ of 57 m/s, the wall design wind speed recommended for 6d wall nails as listed in Table 4 (26%=(42-57)/57×100%). The predicted failures prior to the recommended wall design wind speeds may result from two sources: (1) the unrealistic load assigned to the nail by the tributary area method based on the stud spacing and the spacing of the interior fasteners in the conventional design procedure; and (2) the underlying assumption that neglects the impacts of global frame deformations on the nail responses. These two simplifications in the design philosophy may be responsible for the underestimation of the structural responses to the realistic wind loads. In comparison, FEM is more realistic in resolving these two points.

Using the nail type with a high withdrawal capacity is an effective mitigation measure to raise

the first failure wind speed. As listed in Table 4, a ring shank nail has a capacity of 400 N that is 3.8 times the capacity of a plain nail, 103 N, when fastening the 11 mm OSB wall panel under the wet condition. This increases the first failure wind speed by 96% (from 58 m/s to 114 m/s) for roof nails and 94% (from 38 m/s to 74 m/s) for wall nails.

3.4 Nail head pull-through

The nail head pull-through is another dominant failure mode observed in wood panels when the sheathing bearing perpendicular to the plane of plies fails (FEMA 2005). The resistance of the nail head pull-through is apparently influenced by the panel thickness based on the capacity expression $y=160.48x\text{-}181.58$, where y is the pull-through strength and x is the panel thickness (Herzog and Yeh 2006). The service condition (dry or wet) is another factor that has impacts on the nail head pull-through capacity. The ratio of the mean capacity for the wet exposure condition over that for the dry case is 0.86 for the 13 mm plywood sheathing attached to a southern pine lumber by 8d box nails (3mm × 63.5 mm with a head diameter of 7.5 mm) according to Herzog and Yeh (2006). In their laboratory testing, nails were driven into the specimens prior to 24-hour water soak and the specimens were tested immediately upon the removal from water. Conventionally, the nail head pull-through reactions might not be checked in most designs involving fastener performance. The nail head pull-through capacities for two sheathing types (13 mm plywood panel and 11mm OSB panel) under both dry and wet conditions are listed in Table 5 along with the first failure wind speeds for the roof nails and wall nails.

Table 5 Nail pull-through capacities and corresponding first failure wind speeds

Sheathing type	Service condition	Capacity (N)	First failure wind speed (m/s)		Design wind speed [a] (m/s)
			roof	Wall	wall
1/2 in. (13 mm) plywood	Dry	313	107 (98)[b]	68 (63)	66
	Wet	269	102 (94)	63 (58)	
7/16 in. (11 mm) OSB	Dry	227	95 (87)	61 (56)	
	Wet	195	85 (78)	56 (51)	

a. "Design wind speed" is converted from 3 second gust wind speed at the mean roof height of 9.14 m (30 ft) used in APA (2012) to 10 m to be consistent with ASCE 7-10 wind speed, e.g., $66=65\times(10/9.14)^{(1/6.075)}$.

b. The wind speeds are $\hat{U}^{Open}_{3s,10m}$ ($V^{Water}_{1min,10m}$).

Similar to the nail withdrawal failure mechanism, the first nail head pull-through failure occurs at the corner edge of the leeward wall where the maximum nail stretch develops. The nail heads start to punch the roof sheathing at $\hat{U}^{Open}_{3s,10m}$ = 85 to 107 m/s ($V^{Water}_{1min,10m}$ = 78 to 98 m/s), about 55% higher than the initial damage wind speeds for wall nails ($V^{Water}_{1min,10m}$ = 51 to 63 m/s). An increase of the panel thickness is an effective way to mitigate the pull-through failure. The 2 mm increment in the panel thickness raises the nail head pull-though capacity by 38% (227 N to 313 N for the dry

service condition and 195 N to 269 N for the wet condition in Table 5). Consequently, this increase enhances the sheathing panel to resist at least 13% higher wind speed (87 m/s vs. 98 m/s under the dry condition and 78 m/s vs. 94 m/s under the wet condition).

As also seen in Table 5, except for the case with the highest capacity, i.e., the 13 mm plywood panel under the dry condition, the predicted first failure wind speed for the wall nails ($\hat{U}_{3s,10m}^{Open} =$ 56 to 63 m/s) is 3% to 15% lower than the design wind speed of 66 m/s for the remaining three cases with a thinner panel thickness (11 mm) or under wet conditions. This implies that the capacity of the wall sheathing panel is somehow overestimated by APA (2012), especially for the cases with a thinner panel thickness. Compared to the first failure wind speeds predicted for the nail withdrawal failure, the nail head pull-through failure occurs at a 27% higher wind speed for the plain shank nail connection, 13 mm plywood wall under the dry condition ($V_{1min,10m}^{Water} = 63$ m/s vs. 49 m/s). This means that the nail withdrawal failure occurs prior to the nail head pull-through and thus controls the worst case in this particular case. However, a check of the nail head pull-through limit state still has a practical meaning in evaluating the building envelope performance, since the nail head pull-through may control the worst case due to the uncertainties in the material strengths and different geometries.

3.5 Nail load-slip

The nail load-slip is caused by the in-plane (i.e., a roof plane or wall plane) forces transmitted to the individual nail that may fail either in a ductile mode (i.e., the nail pullout) or a brittle mode (i.e., the nail failure in timber members or a nail head punching through a sheathing edge). Extensive research was done on the role of the nail load-slip capacity in governing the overall performance of shear walls, including their strengths and stiffness. The strengths and stiffness of the specimens sheathed with plywood and OSB panels were found comparable until the respective ultimate displacement was reached (Shenton *et al.* 1998, Girhammar *et al.* 2004). The loading-to-grain directions and the edge distances between fasteners and their connected sheets or wood members are the two factors that influence the load-slip capacity in a systematic manner (Girhammar *et al.* 2004). The connection response at each relative displacement or slip can be obtained by the load-slip relationship described by a multiple-parameter analytical model or a regressed empirical load-slip relationship (Girhammar *et al.* 2004, Wang *et al.* 2010).

The nail connection subjected to the load parallel to the grain demonstrates 105% load-slip capacity of the case under the loads perpendicular to the grain at a 2d edge distance (Girhammar *et al.* 2004). Here, d is the nail shank diameter. This is in line with the general belief that the parallel to grain strength of wood is higher than the perpendicular to grain strength. The edge distance was observed to increase about 15% the load-slip capacity on average when the edge distance increases from 2d to 4d. However, an additional 1d increment from 4d to 5d in the edge distance was found to reduce the load-slip capacity by 10%. The influence factors of the load directions and edge distances on the load-slip capacities reported by Girhammar *et al.* (2004) are combined with the ultimate nail load-slip capacities obtained by Mi (2004) in the present study. The adjusted load-slip capacities are used here as the failure criteria, since the sheathing, lumber, and the nail connection tested in Mi's laboratory tests are closer to those used in the proposed FEM as noted in Table 2.

The first nail load-slip failure occurs at a relatively high wind speed, i.e., $\hat{U}_{3s,10m}^{Open} = 80$ m/s

($V_{1\min,10m}^{Water} = 74$ m/s) or above as listed in Table 6, for both the roof nails and wall nails. Overall, it can be concluded that there is a limited difference between the performances of the nailed joint loaded parallel and perpendicular to the grain of lumber in terms of nail load-slip failure (as shown in Table 6 the "parallel" "2d" row and the "perpendicular" "2d" row). For example, the 5% higher parallel to grain strength postpones the first load-slip failure wind speed by 2 m/s for both the roof nails (from $V_{1\min,10m}^{Water} = 74$ m/s in the "perpendicular" "2d" row to 76 m/s in the "parallel" "2d" row) and wall nails (from $V_{1\min,10m}^{Water} = 101$ m/s to 103 m/s) as summarized in Table 6. An optimized edge distance is a promising way to mitigate the nail load-slip failure. The first failure wind speed was increased by 7 m/s and 11 m/s for roof nails and wall nails, respectively, when the edge distance increased from 2d to 3d (a 3.4 mm increment). The same increment in the edge distance only raises the first failure wind speed for both roof and wall nails by 2 m/s for the increase from 3d to 4d, but reduces the first failure wind speed by 2 m/s for the increase from 4d to 5d. It is noted here that while panel failures in uplift is a critical failure mode observed in post-storm studies, the present study is focused on initial failures of nails. Predictions of the entire panel uplift failure need to consider the necessary combined nail failures, which will be included in a future study of progressive failures.

3.6 Sheathing shear

There are two types of shear failures considered for the design of plywood sheathing panels with the cross-laminated construction, including shear through the thickness and rolling shear (APA 1997). The two shear failure mechanisms are discriminated by the force direction. For the shear through the thickness case, the shear force is perpendicular to the sheathing panel, i.e., acting through the total thickness of the multiple pliers and its resulting shear stress corresponds to the transverse shear stress "SYZ" or "SXZ" output by the Shell 93 element in ANSYS (2009). The other shear type, rolling shear, is caused by a pair of shear forces parallel to the sheathing panel, acting in opposite directions and on different ply layers, i.e., the top ply and the bottom ply. Its numerical counterpart is the in-plane shear stress "SXY" predicted by the Shell 93 element (ANSYS 2009). The allowable strength for the shear through the thickness case is chosen as 1.07 MPa as listed in Table 2. Meanwhile, the allowable rolling shear (in-plane shear) strength is chosen as 0.43 MPa as specified for the plywood of "Structural-1 Grade Stress Level" under "Wet condition" in APA (1997). Thus, the rolling shear strength is 40% of the strength for the shear through the thickness case (0.43MPa/1.07MPa = 40%). It is noted that since in most cases hurricanes bring heavy rain, the wooden members may be exposed to significant rain if the roof shingles had failed. Though one can argue that the wood may not become sufficiently saturated with water over a relative short duration of the storm to match the wet condition reported in the laboratory test, it is on the conservative side to choose the material properties under wet conditions.

The first failure wind speeds for the shear through the thickness case are $\hat{U}_{3s,10m}^{Open} = 61$ m/s ($V_{1\min,10m}^{Water} = 56$ m/s). However, the rolling shear failure is initialized at lower wind speeds of $\hat{U}_{3s,10m}^{Open} = 42$ m/s ($V_{1\min,10m}^{Water} = 38$ m/s). As discussed earlier, the first nail withdrawal failure occurs

at $\hat{U}_{3s,10m}^{Open} = 46$ to 54 m/s ($V_{1min,10m}^{Water} = 42$ to 49 m/s) for the plain shank nail fastening the 13 mm plywood sheathing. Therefore, it may be concluded that the nail withdrawal and the rolling shear of sheathing panels are the two early failure modes. This agrees with the findings by Thampi *et al.* (2011) on the numerical predictions for a low-rise residential building under a tornado event. In the rolling shear case, i.e., the control case, the first failed shell elements are on the windward roof where the plywood panels are nailed to the gable end wall. It is expected that more shell elements will exceed the rolling shear strength (0.43 MPa) with the increase in the wind speed. The emerging new damaged shell elements scatter at or near the nailing spots, which reinforces the fact that the building envelope is essentially governed by the connection details.

Table 6 Nail load-slip capacities and corresponding first failure wind speeds

Load-to-Grain directions	Edge distances	Capacity (N)	First failure wind speed (m/s)	
			Roof	wall
Parallel	1d	995	80 (74)[a]	107 (98)
	2d	1073	83 (76)	110 (101)
Perpendicular	2d	988	80 (74)	107 (98)
	3d	1297	88 (80)	119 (110)
	4d	1381	90 (83)	122 (112)
	5d	1244	88 (80)	119 (110)

a. The wind speeds are $\hat{U}_{3s,10m}^{Open}$ ($V_{1min,10m}^{Water}$).

3.7 Sheathing bending and axial reactions

The axial strength and bending strength are specified separately in APA (1997) and both strengths under the "Wet condition" are selected in the current section as the thresholds to consider the capacity reduction due to the hurricane-induced heavy rain as discussed earlier. The building envelope is not observed to fail due to the two-way bending action up to $\hat{U}_{3s,10m}^{Open} = 83$ m/s ($V_{1min,10m}^{Water} = 76$ m/s, Category 5 hurricane). At $\hat{U}_{3s,10m}^{Open} = 83$ m/s, the maximum bending stress only reaches 20% of the allowable bending capacity. The maximum bending stresses occur at the second lowest sheathing panel located between the intermediate supports on the leeward roof.

No sheathing damage due to the axial forces is observed from Category 1 to 5 hurricane scale and the tensile stresses accumulate most significantly on the roof edge along the gable ends, reaching 43% of the axial strength at $\hat{U}_{3s,10m}^{Open} = 88$ m/s ($V_{1min,10m}^{Water} = 80$ m/s). The outputs of the axial stresses are taken from the mid-surface of the shell elements to show the membrane results only. The bending stresses are the differences between the axial stresses at the top or the bottom surface and the mid-surface axial stresses.

3.8 Initial wind speeds associated with seven failure mechanisms

The failure criteria for all the seven discussed failure mechanisms along with the corresponding first failure wind speeds are summarized in Table 7. The rolling shear, the nail withdrawal, the excessive displacement of sheathing, the nail head pull-through, the sheathing shear through the thickness, and the nail load-slip are found to be responsible for the building envelope damage. The building envelope has adequate bending and axial strengths since no damage appears in the predictions up to $\hat{U}^{Open}_{3s,10m} = 139$ m/s ($V^{Water}_{1\min,10m} = 127$ m/s), which agrees with the conclusions drawn by Frühwald *et al.* (2007) who investigated 127 failure cases of wood structures from 8 countries. It was concluded that the wood quality and production methods are only responsible for a small part (together about 11%) of all the investigated failures. The dominating reasons behind the failure events were found to be related to the insufficient design with respect to mechanical loadings (41%). For an instance, the absent or inadequate nailing of sheathing was one triggering cause for the complete roof collapse for a recital hall with a span of 24 m as reported in Case 20 by Frühwald *et al.* (2007).

Table 7 The first failure wind speeds associated with 7 failure mechanisms for building

Failure mechanism	Failure criteria	First failure wind speed (m/s)	Damage location
Rolling shear	Sheathing in-plane shear stress	42 (38)[a]	Windward roof nailed to gable end walls
Nail withdrawal	Nail axial reaction	46 (42)	Corner edge of the leeward wall
Sheathing disp.	L/120	51 (47)	Leeward roof edge near overhang
Nail head pull-through	Nail axial reaction	56 (51)	Corner edge of the leeward wall
Shear through the thickness	Sheathing transverse shear stress	61 (56)	Corner edge of the windward side wall
Nail load-slip	Nail shear reaction	74 (80)	Leeward roof edge
Sheathing bending	Extreme fiber bending strength	127+	N/A
Sheathing tension/compression	Sheathing axial strength	127+	N/A

a. The wind speeds are $\hat{U}^{Open}_{3s,10m}$ ($V^{Water}_{1\min,10m}$).

4. Conclusions

A refined 3D FEM with in-depth construction details is developed and analyzed to evaluate the building envelope performance that is the primary reason for the hurricane loss but not well addressed so far. The following conclusions are formed based on the discussions of the seven failure mechanisms of the building envelope for a typical 5:12 sloped gable low-rise building under the given wind tunnel load case at a wind angle of 90 degrees. It is noted that this is different from a typical building design that needs to consider all wind attack angles from 0 to 360 degrees. The present study is focused on developing a numerical procedure to investigate the envelope performance under a given load condition.

1. The predicted potential damage zones based on the Von-Mises stress are the roof edge sheathings, the gable end walls, and the side wall corners, which agrees qualitatively well with some of the observed failures caused by Hurricane Andrew and Katrina;

2. The worst localized suction determines the maximum envelope displacement up to 67 m/s ($V_{1\min,10m}^{Water}$), while the frame system responses to the overall wind loads shift the maximum envelope displacement to where the maximum lumber frame displacement occurs for 67 m/s and above ($V_{1\min,10m}^{Water}$);

3. The nail stretch, i.e., the relative displacement between the lumber frame and the sheathing panel at the nail spot, determines a nail reaction instead of the localized high wind suctions or the frame deformation to trigger the nail withdrawal failure. The wall design wind speed recommended by the APA (2012) overestimates the initial failure wind speed by 27% on average for the plain nail due to the load distribution using the tributary area method and the neglect of the frame deformations. The ring shank nail with the additional shear resistance provided by the annularly threaded rings can significantly increase the first failure wind speed;

4. The nail head pull-through failure occurs after the nail withdrawal failure. The wall design wind speed recommended by APA (2012) somehow overestimates the initial wind speed for the nail head pull-through failure. An increase of the sheathing panel thickness is an effective way to increase the first failure wind speed for this failure mode;

5. The localized high suctions can initialize the first nail load-slip failure at a very low wind speed. The load-to-grain direction does not significantly impact the first failure wind speed while the optimized edge distance has the potential to postpone the first load-slip failure;

6. The rolling shear of sheathing panels is another early failure mode besides the nail withdrawal, excessive displacement, and nail head pull-through for the building envelope performance. The damaged roof sheathing portions scatter at or near the nailing spots, which reinforces the fact that the building envelope is essentially governed by the connection details;

7. No sheathing damage due to the bending or axial forces is observed for the Category 1 to 5 hurricane scale, which reinforces the fact that the wood quality itself is not the primary reason for the envelope damage.

The present work focuses to clarify when and where each possible failure mechanism related to the building envelope performance occurs. The discussions demonstrate that the integrity of the building envelope is severely impacted by the connections between the building envelope and the lumber frame. The interferences among those failure modes under cyclical wind loads demand a further study to account for the cumulative damage as how a low-rise building goes through a hurricane event in real life, providing a methodology to study the progressive failure of the

residential houses under hurricane loads.

Acknowledgements

References

ANSYS version 12.1 (2009), (computer software). ANSYS Inc., Cecil Township, PA.

APA. (1997), *PDS-Plywood design specification*, The Engineered Wood Association, Tacoma, WA

APA. (2012), *Wind resistance of wood structural panel sheathed walls*, TT-110B, The Engineered Wood Association, Tacoma, WA.

ASCE. (2010), *Minimum design loads for buildings and other structures*, ASCE7-10, Reston, Va.

Asiz, A., Chui, Y.H. and Smith, I. (2008), *Failure analysis of light wood frame structures under wind load*, CIB-W18 Meeting 41, St. Andrews, Canada, Paper 41-15-5.

Chok, C.V. (1988), *Wind parameters of Texas Tech University field site*, M.S. thesis, Texas Tech University, Lubbock, TX.

Cope, A. (2004), *Vulnerability of low rise buildings to hurricane*, Ph.D. Dissertation, University of Florida, Gainesville, FL.

Cramer, S.M., Drozdek, J.M. and Wolfe, R.W. (2000), "Load sharing effects in light-frame wood-truss assemblies", *J. Struct. Eng. - ASCE*, **126**(12), 1388-1394.

Dao, T. and van de Lindt, J. (2008), "New nonlinear roof sheathing fastener model for use in finite-element wind load applications", *J. Struct. Eng. - ASCE*, **134**(10), 1668-1674.

Falk, R. and Itani, R. (1989), "Finite element modeling of wood diaphragms", *J. Struct. Eng. - ASCE*, **115**(3), 543-559.

FEMA. (1992), *Building performance Hurricane Andrew in Florida–Observations, recommendations and technical guidance*, FEMA488, Washington, DC, 28.

FEMA. (2006), *Mitigation assessment team report: Hurricane Charley in Florida*, FEMA488, Washington, DC, 5-1-5-13.

Frühwald, E., Serrano, E., Toratti, T., Emilsson, A. and Thelandersson, S. (2007), *Design of safe timber structures –How can we learn from structural failures in concrete, steel and timber?*, TVBK-3053, Lund, Sweden, Lund, Sweden.

Girhammar, U.A., Bovim, N.I. and Källsner, B. (2004), "Characteristics of sheathing-to-timber joints in wood shear walls", *Proceedings of the 8th World conference on timber engineering*, Lahti, Finland.

Herzog, B. and Yeh, B. (2006), "Nail withdrawal and pull-through strength of panels", *Proceedings of the 9th world conference on timber engineering*, Curran Associates, Inc., Portland, Oregon.

Holmes, J.D. (2001), *Wind loading of structures*, Spon Press, New York, NY, 128-138.

IBC. (2011), *2012 International Building Code*, ICC, Washington, DC

Martin, K.G. (2010), *Evaluation of system effects and structural load paths in a wood-framed structure*, M.S. thesis, Oregon State University, Corvallis, OR.

Martin, K.G., Gupta, R., Prevatt, D.O., Datin, P.L. and Lindt, J.W.v.d. (2011), "Modeling system effects and structural load paths in a wood-framed structure", *J. Architect. Eng.*, 17(4), 134-143.

Mi, H. (2004*), Behavior of unblocked wood shearwalls*, Master, University of New Brunswick, Fredericton, NB.

Pan, F., Cai, C.S. and Zhang, W. (2103), "Wind-induced internal pressures of buildings with multiple openings", *J. Eng. Mech. - ASCE*, **139**(3), 376–385.

Pinelli, J.P., Simiu, E., Gurley, K., Subramanian, C., Zhang, L., Cope, A., Filliben, J.J. and Hamid, S. (2004), "Hurricane damage prediction model for residential structures", *J. Struct. Eng. - ASCE*, **130**(11), 1685-1691.

Shenton III, H.W., Dinehart, D.W. and Elliott, T.E. (1998), "Stiffness and energy degradation of wood frame shear walls", *Can. J. Civil Eng.*, **25**(3), 412-423.

Simiu, E., Vickery, P. and Kareem, A. (2007), "Relation between saffir–simpson hurricane scale wind speeds and peak 3-s gust speeds over open terrain", *J. Struct. Eng. - ASCE*, **133**(7), 1043-1045.

Solari, G. and Kareem, A. (1998), "On the formulation of ASCE7-95 gust effect factor", *J. Wind Eng. Ind. Aerod.*, **77-78**, 673-684.

Thampi, H., Dayal, V. and Sarkar, P.P. (2011), "Finite element analysis of interaction of tornados with a low-rise timber building", *J. Wind Eng. Ind. Aerod.*, **99**(4), 369-377.

Van de Lindt, J., Graettinger, A., Gupta, R., Skaggs, T., Pryor, S. and Fridley, K. (2007), "Performance of wood-frame structures during Hurricane Katrina", *J. Perform. Constr. Fac.*, **21**(2), 108-116.

Wang, Q., Chui, Y.H., Ni, C., Smith, I. and Asiz, A. (2010), "An empirical model to predict load-slip response of laterally loaded nailed joint", *Proceedings of the 11th World Conference on Timber Engineering*, June 20-24, Riva del Garda, Italy.

Wolfe, R.W. and McCarthy, M. (1989), *Structural performance of light-frame roof assemblies: I. Truss assemblies with high truss stiffness variability*, FPL-RP-492, Forest Products Laboratory, Madison, WI.

JH